Nanoscale

REVIEW

View Article Online
View Journal | View Issue

Cite this: *Nanoscale*, 2023, **15**, 18156

Acoustic platforms meet MXenes – a new paradigm shift in the palette of biomedical applications

Bartholomew Richard, [a,b] C. Shahana,[c] Raju Vivek,[d] Amarendar Reddy M.[e] and P. Abdul Rasheed *[a,b]

Received 28th September 2023,
Accepted 30th October 2023

DOI: 10.1039/d3nr04901a

rsc.li/nanoscale

The wide applicability of acoustics in the life of mankind spread over health, energy, environment, and others. These acoustic technologies rely on the properties of the materials with which they are made of. However, traditional devices have failed to develop into low-cost, portable devices and need to overcome issues like sensitivity, tunability, and applicability in biological *in vivo* studies. Nanomaterials, especially 2D materials, have already been proven to produce high optical contrast in photoacoustic applications. One such wonder kid in the materials family is MXenes, which are transition metal carbides, that are nowadays flourishing in the materials world. Recently, it has been demonstrated that MXene nanosheets and quantum dots can be synthesized by acoustic excitations. In addition, MXene can be used as a mechanical sensing material for building piezoresistive sensors to realize sound detection as it produces a sensitive response to pressure and vibration. It has also been demonstrated that MXene nanosheets show high photothermal conversion capability, which can be utilized in cancer treatment and photoacoustic imaging (PAI). In this review, we have rendered the role of acoustics in the palette of MXene, including acoustic synthetic strategies of MXenes, applications such as acoustic sensors, PAI, thermoacoustic devices, sonodynamic therapy, artificial ear drum, and others. The review also discusses the challenges and future prospects of using MXene in acoustic platforms in detail. To the best of our knowledge, this is the first review combining acoustic science in MXene research.

1. Introduction

Sound signal perception has been monitored by mankind for decades, and the term 'acoustics' deals with the production, transmission, control, and effects of sound. It is a physical science closely related to our daily lives in the form of telephonic conversations, sound absorption systems, ultrasound imaging, voice interaction systems, and others. According to the definition of sound, it is a vibration that propagates as an acoustic wave through a transmission medium, such as a gas, liquid, or solid, and an acoustic wave is a mechanical wave that transmits energy through the movements of atoms and molecules.[1] A sound wave is typically investigated in terms of its pressure levels, frequencies, and interactions with the environment. This interaction can be labelled as diffraction, interference, reflection, a combination of these three, or even refraction when it involves many media. Since the sound source causes the medium it is in to vibrate, the sound wave spreads out from the source and disperses energy throughout the medium. This energy is converted into new forms at the location of the reception such as physical, biological, or other effects.[2]

Acoustic waves (sound) are mechanical vibrations that travel through elastic media like air, liquid, or solid objects. Acoustic waves are referred to as audible sound, ultrasonic, and infrasonic by separating the complete spectrum into three parts. The only range of sound that can be recognized by human ears is the audible range, which is roughly between 20 Hz and 20 kHz. Over 20 kHz is considered as the ultrasonic range and this frequency range is employed in medical applications, such as ultrasonography because the shorter wavelengths improve the imaging resolution.[3] A suitable transducer that can convert electrical energy or other forms of energy to acoustic energy is typically used to generate ultrasound.[4] The

[a]*Department of Biological Sciences and Engineering, Indian Institute of Technology Palakkad, Palakkad, Kerala, 678557, India. E-mail: abdulrasheed@iitpkd.ac.in*
[b]*Department of Chemistry, Indian Institute of Technology Palakkad, Palakkad, Kerala, 678557, India*
[c]*Department of Chemistry, National Institute of Technology Calicut, Calicut, Kerala, 673601, India*
[d]*Bio-Nano Theranostic Research Laboratory, Cancer Research Program (CRP), School of Life Sciences, Bharathiar University, Coimbatore, 641 046, India*
[e]*Department of Chemistry, School of Sciences, National Institute of Technology Andhra Pradesh, West Godavari, Andhra Pradesh, 534101, India*

majority of ultrasonic transducers make the use of piezoelectric materials and the opposing piezoelectric effect to produce acoustic waves from an alternating electric field. The final segment, or 20 Hz and lower, is where the infrasonic range is located.

The first large-scale application of ultrasound occurred towards the start of World War I (1914), with the development of the first underwater sound navigation and ranging system (known as SONAR), which relied on a pulse-echo operation.[5] Many additional uses for ultrasound emerged in the years afterward, encouraging the advancement of new technological improvements. As a form of physical treatment, ultrasonography was used in the 1930s to generate heat and warm the deep tissues in the body. Ultrasonic pulse-echo imaging was developed and deployed to diagnostic medicine in the late 1940s to lessen reliance on radiative medical X-ray imaging.[6] In the 1950s, Fellinger and Schmid effectively used ultrasonic irradiation to promote the transport of hydrocortisone ointment into inflamed tissues for the treatment of polyarthritis.[7] Since then, the discipline of diagnostic and therapeutic ultrasound, often known as medical ultrasound, has evolved into one of the most active research areas, with numerous notable breakthroughs documented. Ultrasound imaging has been widely and actively employed in the fields of cardiology, gynaecology, angiology, and gastroenterology due to its benefits such as ease of use, low cost, noninvasive assessment, and the absence of ionizing radiation.[8–10] Furthermore, ultrasound has been used to increase drug or gene delivery into specific tissues such as the brain, skin, and endothelium. It has also been used to treat a variety of disorders, including thromboembolism, cancer, and arteriosclerosis.

Acoustic waves have been used for decades in biological sciences and engineering, with applications ranging from disease diagnostics, including imaging techniques to high-energy sound wave lithotripsy. Acoustic waves can manipulate the fluid flow in the micro and nanoscale, which can be used to develop miniaturized technologies and microelectromechanical systems (MEMS).[11] This domain of contactless and label-free acoustic technique is known as acoustofluidics,[12] and its applications range from the analysis of cells,[13] and biomolecules,[14] to techniques like acoustic levitation,[15] acoustic actuation,[16] acoustophoresis,[17] acoustic tweezers,[18] *etc*. Recent progress in acoustofluidics technologies for diagnostics, drug synthesis and delivery, tissue engineering, fundamental biological studies, biological particle separation, and sorting proves the evidence of using acoustics in modern medical science and technology.[19]

At the beginning of the 1980s, nanoscience and technology received greater attention among a broad spectrum of the research community. In the past decades, nanotechnology served as a platform for the multidisciplinary research of collections like chemistry, material science, physics, biology, and medicine. In many ways, the blend of nanotechnology and ultrasound for biomedical applications has revolutionized conventional techniques to apply ultrasound. Even the integration of nanotechnology and acoustics has led to a new branch of study called 'nanoacoustics' that deals with the study of the manipulation of nanomaterials with acoustics and its various applications like nanoacoustic characterization, nanoacoustic sensing, ultrasound drug delivery, PAI, *etc*.[20] Nanomaterials for acoustics were broadly classified as active and passive, lead zirconate titanate (PZT),[21] polyvinylidene difluoride (PVDF) nanofibers,[22] *etc*. belong to active while organic nanomaterials (such as organic molecules[23] and semiconducting nanomaterials[24]) and inorganic nanomaterials (such as metallic nanoparticles,[25] metallic nano-patterns,[26] and carbon-based nanomaterials[27]). Active nanomaterials for acoustics can generate an electrical field when acoustic waves strike them, or they can generate acoustic waves in the presence of an electrical or magnetic field, whereas passive nanomaterials for acoustics primarily consist of nano-scaled materials that aid in acoustic generation/detection and interact with acoustic waves for different purposes.

The advent of two-dimensional nanomaterials in the palette of materials science has made a notable change in applications like biomedical,[28] energy[29] as well as the environment sector.[30] When these materials were integrated into the acoustics field, advancement in different application sectors

Bartholomew Richard

Bartholomew Richard received his Master's degree in Chemistry from Fatima Mata National College (Autonomous), University of Kerala, India, in 2022. His research area is focused on exploring 2D materials and their composites for biomedical applications. He is currently working on developing MXene-based composites for fabricating flexible and wearable sensors for the real-time monitoring of bioanalytes.

C. Shahana

Shahana C. received her Master of Science in Chemistry from the National Institute of Technology Calicut, Kerala, India. Her research interest mainly focuses on exploring the biomedical applications of 2D materials like developing wearable and flexible biosensors.

was quoted by the materials scientists. Materials like graphene,[31] reduced graphene oxide,[32] transition metal oxides,[33] transition metal dichalcogenides,[34] metal–organic frameworks (MOF),[35] covalent organic frameworks,[36] hexagonal boron nitride (h-BN),[37] black phosphorus[38] and MXenes[39] showed a wide variety of advances when integrated with acoustics. These materials have been used in acoustic sensing, photoacoustic imaging (PAI), thermoacoustic devices, *etc*. Out of these materials, MXenes being the youngest family member has recently been explored in the acoustics domain. This family of transition metal carbides has already explored applications in biosensing,[40,41] wastewater treatment,[42] cancer therapy,[43] energy storage,[44] electromagnetic interference (EMI) shielding,[45] biomedical applications[46] *etc*. In this review, we have briefly elucidated the synthetic techniques and the biomedical applications of MXenes using acoustics platform. As per the best part of our knowledge, this is the first review article covering the integration of MXenes and acoustic platforms for biomedical applications.

2. Introduction to MXenes

MXenes are a new class of two-dimensional materials of transition metal carbides or carbonitrides with the general formula $M_{n+1}X_nT_x$ (n = 1–4 layers) in which M represents early transition metal, which is inserted between carbon/nitrogen (X) and T_x represents surface terminations such as –O, –OH, and –F.[47] A large variety of compositions and structures are possible in the MXene family by varying the combination of transition metals, carbon/nitrogen, and functional groups.[48] It has been reported that over 100 stoichiometric MXene compositions with unique functionalities make MXenes suitable for multiple applications.[49,50] The fascinating properties of MXenes include excellent conductivity,[51] hydrophilicity,[52] catalytic activity,[53] easy functionalization,[54] good biocompatibility,[55] and the ability to form robust films.[56] Among the large family of MXenes, $Ti_3C_2T_x$ MXene is largely explored for different applications, including acoustic applications.[57,58] However, other MXenes such as Nb_2CT_x, Mo_2CT_x, and $Ta_4C_3T_x$ are also explored for various applications including acoustic applications.[59,60]

The synthetic routes of MXenes mainly revolve around three different etching methods for removing the A layer from their corresponding MAX phases. The first and most commonly employed method is the hydrofluoric acid (HF) etching method by reacting the MAX phase in 48% HF for several hours (varies 24–96 h) at room temperature. The major issue with this method is that HF is a highly corrosive and toxic acid that can cause burns and damage to the skin upon contact. Another etching method involves the *in situ* generation of HF produced by mixing lithium fluoride (LiF) with hydrochloric acid (HCl), which is less hazardous. The *in situ* HF etching method is highly successful for the etching of Ti-based MXenes; however, it is not highly recommended for Nb-based MXenes owing to the stronger Nb–Al bond strength than Ti–Al. Another etching method is an alternative to the use of toxic etchants, replacing it with a mixture of $NaBF_4$ and HCl with a comparatively shorter time duration (30 h).[61] This etching route can be considered an environmentally benign route for MXene synthesis with high exfoliation efficiency in addition to better chemical and oxidative stability, enhanced conductivity, and lower cytotoxicity. Recently, new synthetic methodologies have evolved, which include the use of HCl as the etchant[62,63] and electrochemical etching methods.[64] After successful etching, the next step is to exfoliate the multilayer MXene

Raju Vivek

Raju Vivek is currently working as Assistant Professor (designated as DBT-Ramalingaswami Re-entry Fellow of Govt. of India) at Bharathiar University, India. He is now proceeding with his research in the Cancer Research Program and is the Head of Bio-Nano Theranostics Research Laboratory at Bharathiar University. He took two terms of postdoctoral research in the School of Biomedical Engineering at Shanghai Jiao Tong University, China. Then, he moved to further postdoctoral research at the Rajiv Gandhi Centre for Biotechnology, Kerala. His research focuses on the engineering design, synthesis, and multimodal biomedical nanomaterials for the applications of molecular imaging contrast agents, stimuli-responsive programmed targeting drug delivery systems, and activatable theranostics.

Amarendar Reddy M.

Amarendar Reddy M. is an Assistant Professor in the Department of Chemistry, School of Sciences, National Institute of Technology Andhra Pradesh, India. He obtained his PhD degree in Chemistry from the Indian Institute of Science Education & Research, Bhopal, India. His research area includes biomaterials, biosensors, self-assembled nanostructures, and bioinformatics.

sheets into delaminated sheets (single- to few-layer MXene sheets). Mechanical exfoliation is quite challenging because of the hydrogen bonding between MXene layers.[65] To avoid this, intercalation of different solvents, organic molecules, and ions between the MXene layers, followed by agitation or sonication can be used, which can expand the interlayer spacing and minimize the interflake interactions.[66]

Recently, it has been demonstrated that MXene nanosheets and quantum dots (QDs) can be synthesized by acoustic excitations, which is discussed in the next section.[67–69] In addition, MXene can be used as a mechanical sensing material for building piezoresistive sensors to realize sound detection as it produces a sensitive response to pressure and vibration. This efficient mechanical response of MXenes originated by changing the interlayer distances with an applied force.[39] It has been demonstrated that MXene nanosheets show high photothermal conversion capability, which can be further established as the photothermal nanoagents for cancer treatment.[70] This high photothermal conversion capability of MXenes provides contrast-enhanced imaging capability, which can be utilized in PAI. Fig. 1 shows the various biomedical applications of MXenes using an acoustic platform.

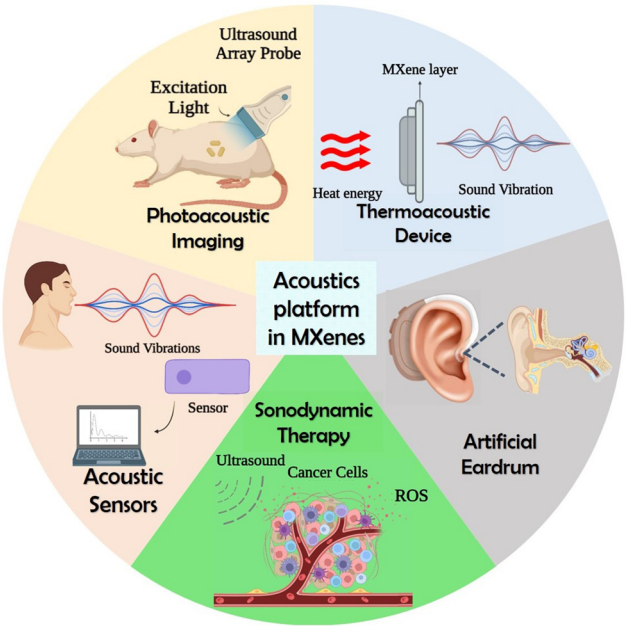

Fig. 1 Schematic representation showing the acoustic applications of MXene, created with BioRender.com.

3. Acoustics in MXene synthesis

Ghazaly *et al.* introduced a novel one-step salt solution-based acoustic synthesis method for converting the Ti_3AlC_2 MAX phase into $Ti_3C_2T_x$ MXene, which involved the use of megahertz acoustic excitation to generate protons *via* solution dissociation.[69] They employed 30 MHz high-frequency energetic surface acoustic waves (SAWs) and the influence of the evanescent electric field (108 V m^{-1}) interacted with a droplet consisting of 0.05 M LiF solution containing Ti_3AlC_2 MAX particles. The SAW process harnessed the high localization of mechanical vibrations to facilitate rapid water dissociation and proton evolution upon exposure to acoustic waves. The strong electromechanical coupling properties of the piezoelectric substrates facilitated a dynamic polarization process at atomic and molecular scales, leading to the exfoliation of the bulk MAX phase into one or more layers of nanosheets. The $Ti_3C_2T_z$ MXene formation mechanisms are suggested to follow the below equations.

Water dissociation:

$$SAW + H_2O \rightleftharpoons H^+ + OH* + e^-$$

Localized HF formation:

$$LiF + H^+ \rightleftharpoons HF + Li^+$$

Delaminated MXene production:

$$Ti_3AlC_2 + aHF + bH_2O \rightarrow Ti_3C_2T_z + AlF_3 \cdot xH_2O + cH_2.$$

Acoustic waves improve mass transfer by inducing acoustic streaming throughout the entire solution volume. This effect results in increased exposure of additional active sites to the etching solution. This mechanism accelerates the overall process while also ensuring a uniform distribution of MXene flakes in terms of their size. The SAWs facilitate the dissociation of water molecules, producing OH* free radicals and protons (H^+). The protons then react with fluorine ions to form localized hydrofluoric acid (HF), causing a slight decrease in the solution's pH. This decrease in pH extends the solubility limit of LiF at room temperature, enabling it to reach the minimum concentration required to etch out the aluminium layer. The OH* free radicals play a role in the formation of surface termination groups on the MXene. This rapid reaction technique not only eliminated the need for acids but also

P. Abdul Rasheed

P. Abdul Rasheed received his PhD degree from the School of Nano Science and Technology, National Institute of Technology Calicut, India, in 2015. After his PhD, he did postdoctoral fellowships at Korea University, South Korea, and Qatar Environment and Energy Research Institute, Doha, Qatar. Currently, he is a Ramalingaswami Fellow at the Department of Biological Sciences and Engineering at the Indian Institute of Technology Palakkad, India. His research interests are electrochemistry, nanomaterial-based biosensors, wearable sensors, MXenes and other 2D materials, biomarkers for neurological disorders, and biomedical engineering.

demonstrated its potential for large-scale MXene synthesis. Additionally, the presence of Li ions becomes confined between the multi-layered MXene, contributing to the delamination of MXene flakes. The high-frequency SAW is believed to significantly enhance the kinetic rates of the reaction, while the mechanical wave component generated by the SAW facilitates the delamination process. Recently, Alijani *et al.* developed a unique method for creating MXene quantum dots (MQDs) based on an acoustomicrofluidic approach with minimal degradation.[68] The schematic illustration of the experimental setup is given in Fig. 2, in which a multilayer $Ti_3C_2T_z$ MXene sample is continuously brought to the surface-reflected bulk waves (SRBW) device through the formation of aerosol droplets of delaminated and cleaved $Ti_3C_2T_z$, which is finally collected at the bottom of the glass bottle enclosure. As shown in the figure, the piezoelectric substrate's high-frequency electromechanical vibrations greatly speed up the surface, nebulizing the layered $Ti_3C_2T_z$ dispersion and resulting in progressively smaller and thinner MXene nanosheets and MQDs. This room-temperature synthesis method that doesn't require the input of any additional chemicals produced high-purity MXene quantum dots with superior performance as electrode materials for the electrochemical sensing of hydrogen peroxide.[54]

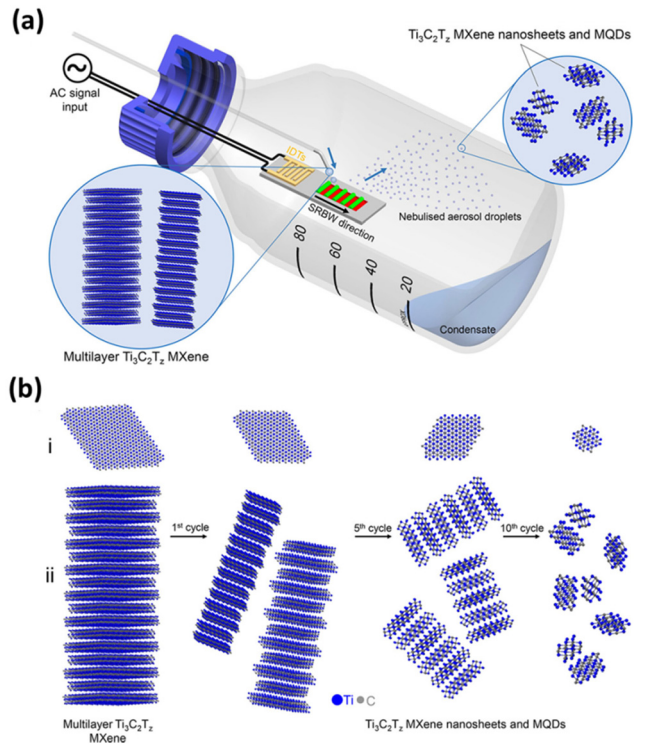

Fig. 2 (a) Schematic illustration of the experimental setup for the acoustomicrofluidic synthesis of pristine ultrathin $Ti_3C_2T_z$ MXene nanosheets and MQDs. Here, the multilayer $Ti_3C_2T_z$ MXene sample is continuously delivered to the SRBW device. The delaminated and cleaved $Ti_3C_2T_z$ condenses within the glass bottle enclosure after forming the aerosol droplets in the top by nebulization. (b) The condensate collected after many cycles at the bottom undergoes successive renebulization to form (i) laterally cleave and (ii) delaminate the sample into smaller and thinner MXene nanosheets and MQDs. Reproduced with permission from ref. 68. Copyright © 2021, American Chemical Society.

4. MXene in acoustic applications

4.1. Artificial eardrum and throat

Human hearing receives air disturbances with periodic pressure changes, which are then translated into sounds by the ear. The auditory system handles human hearing, which transforms the eardrum's mechanical waves into neural pulse responses for brain processing. Presbycusis, which affects older individuals, heredity, congenital abnormalities, and a person's surroundings, can all result in hearing loss. Using a hearing aid and treating the perforated eardrum are two strategies that can improve hearing. Hearing aid devices that combine a microphone, amplifier, and loudspeaker have made life easier for those who are deaf and suffer hearing loss. The major components of a hearing aid include a microphone, which picks up the sound, and an amplifier circuit to enhance the sound. The next is a miniaturized loudspeaker (receiver), which delivers the amplified vibrations to the external acoustic meatus (auditory canal), and the electronic parts are powered by batteries. The general mechanism in the working of a hearing aid is the transport of an input signal to the microphone. This signal gets amplified using a battery-powered amplifier and passed to the receiver in the form of an output signal. Fig. 3 shows the schematic outline of the mechanism of a hearing aid.

Currently, available acoustic technology is restricted by bulky rechargeable nickel–metal batteries that are difficult to carry. Isinglass, wood, mica, and polymers are the usual materials used in conventional acoustic membranes. They are heavyweight and are difficult to tailor. Acoustic devices' ultimate objective is to create or detect a sound with great sensitivity, low limit of detection, and a large frequency spectrum. Core demands for technical innovation include lightweight,

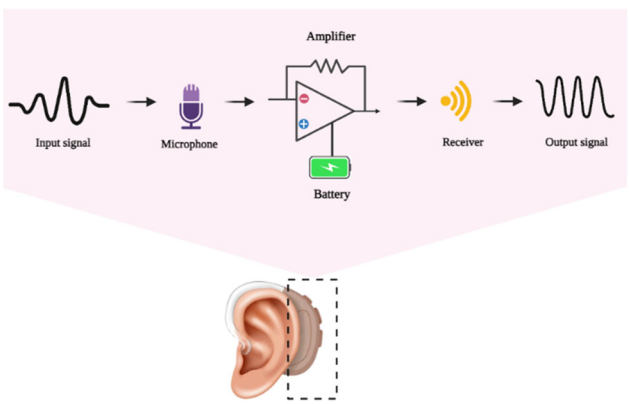

Fig. 3 The general outline mechanism behind the working of the artificial hearing aid, created with BioRender.com.

low energy consumption, battery longevity, and integration with microsupercapacitors or microbatteries. Acoustic membrane performance may be enhanced by nanostructured materials, especially low-dimensional materials.[71] Low-dimensional nanostructures have already been implanted in the damaged eardrum of animal models to restore hearing. Deep data learning-aided speech recognition has been reported to be possible with acoustic sensors built of graphene.[72]

Recently, Ren *et al.* built an artificial eardrum using an acoustic sensor based on $Ti_3C_2T_x$ for realizing voice detection and recognition.[39] The fabricated eardrum mimics the function of a human eardrum, which consists of MXene with a large interlayer distance and micropyramid polydimethylsiloxane arrays, enabling two-stage amplification of pressure and acoustic sensing. The overview of the two-stage amplified MXene artificial eardrum with the operating principle of two-stage enhancement, and the schematic illustration of the MXene eardrum device are given in Fig. 4. The difference between the conventional sensor and MXene-based sensor is given in Fig. 4(a). The device is assembled from double-layer MXene–polydimethylsiloxane (PDMS)–polyethylene (PE) films, abbreviated as MPP film, as shown in Fig. 4(b). The image of the MXene eardrum device, image of the MXene device placed on the ear model, and the fabrication process of the MXene–PDMS–PE film are given in Fig. 4(c–e), respectively. The scanning electron microscopy (SEM) images of the PDMS substrate with pyramid microstructures and the substrate covered with MXene nanoflakes are shown in Fig. 4(f) and (g), respectively.

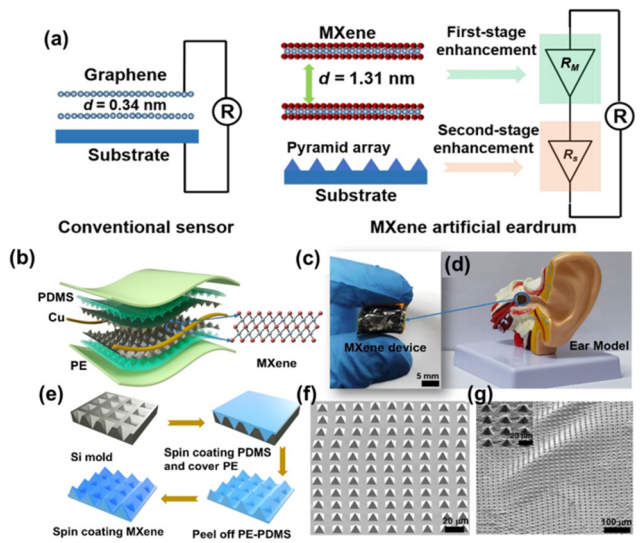

Fig. 4 (a) The operating principle of two-stage enhancement of the fabricated MXene artificial eardrum. (b) Schematic representation of the MXene eardrum device. (c) The image of (c) MXene eardrum and (d) MXene device placed on the ear model. (e) Fabrication process to prepare the MPP film. The SEM image of (f) the PDMS substrate with pyramid microstructures and (g) the substrate covered with MXene nanoflakes. Reprinted with permission from ref. 39. Copyright © 2022 The Authors, some rights reserved; exclusive license American Association for the Advancement of Science.

The fabricated artificial eardrum displays an exceptionally high sensitivity of 62 kPa^{-1} with a promising detection limit of 0.1 Pa. They have adopted a machine-learning model to realize the training and testing of large amounts of data recorded by the fabricated MXene device. The results indicate that the MXene artificial eardrum shows great potential for applications in wearable acoustical healthcare devices in building a human–machine interaction system.

Another interesting work is the fabrication of MXene-based acoustic devices in speech recognition. Towards this aspect, Jin *et al.* fabricated a wearable and deep-learning-enabled MXene-based artificial throat device using $Ti_3C_2T_x$ MXene conductive film and PDMS.[73] This artificial MXene-based sound detector (MXSD) throat device realizes the detection of the action of sound signals at different frequencies and intensities, along with the detection of different pronunciations of several different words. They have combined MXSD with a deep learning network model to further explore the performance of the device in recognizing two sound signals (long vowels and short vowels). They have concluded that the developed MXSD has the potential to become a wearable artificial throat device in biomedical fields that assists patients in communication and the development of deep-learning-enabled sensors in complex data environments.

4.2. Photoacoustic imaging

The photoacoustic effect is a particular case of the thermoacoustic effect, in which the heat energy is generated by the absorption of light by the sample. When the sample is irradiated by a pulse light source (flash) or a modulated light (periodic light) using a laser source, the material absorbs the light energy and converts it into heat energy. These temperature variations, translated into regular pressure changes, are followed by the expansion and contraction of the substance and the surrounding medium. Thus, sound waves are generated and this phenomenon is named as the photoacoustic effect.[74]

The commonly used wavelength for PAI is in the visible and near infrared (NIR) part of the spectrum between 550 and 900 nm. The photoacoustic property is predominantly applied in the field of PAI, which is a cutting-edge diagnostic imaging technique that produces optical imaging by introducing the tissue to the excitation light. This can be used for functional imaging of a biological cell or tissue structure, which can be employed in the early detection and primary stage treatment of cancer. Fig. 5 shows the schematic representation of PAI of tumour cells and the mechanism of action involved during the process. Apart from PAI, the photoacoustic effect can be applied to reproduce sound. For example, few-layer graphene can transform optical energy into sound energy while optical excitations are applied.[75]

PAI utilizes both endogenous and exogenous contrast agents to image cells and tissues. The endogenous agents include DNA,[76] lipid,[77] oxygenated-/deoxygenated-haemoglobin,[78] melanin,[79] *etc.* These contrast agents come up with functional, histopathologic, and metabolic information such as blood oxygenation, vascularity, and oxygen metabolism.

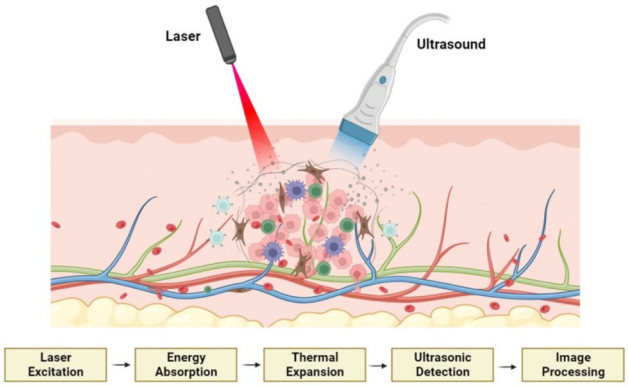

Fig. 5 Schematic representation of PAI of tumour cells and the mechanism of action involved, created with BioRender.com.

Coming to exogenous contrast agents, several materials, including fluorescent proteins (red/green fluorescent protein (RFP/GFP)),[80,81] organic dyes,[82] and inorganic nanomaterials (gold nanoparticles,[83] graphene,[84] carbon nanotubes,[85] mesoporous silica nanoparticles,[86] MOFs,[87] covalent–organic frameworks,[88] MXenes[89] *etc.*), are used as good PAI contrast agents. MXenes, the youngest 2D material, are excellent PAI contrast agents because they can undergo photothermal conversion and span a spectrum from ultraviolet-visible to near-infrared. $Ti_3C_2T_x$, Nb_2CT_x, and $Ta_4C_3T_x$ are the MXenes that demonstrated excellent photoacoustic behaviour combined with photothermal effect or singly, which is evident from the previous literature.

The extensive surface area and ultrathin planar structure of MXene sheets provide numerous binding sites for therapeutic drugs, along with high photothermal and photoacoustic conversion efficiency.[89] Wang *et al.* synthesized 3-bromopyruvate-loaded $Ti_3C_2T_x$ MXene/Cu_2O nanosheets for PAI-guided synergistic cancer therapy combined with photothermal therapy (PTT)/chemodynamic therapy (CDT).[89] The composite contains Cu^+, which produces OH* radical *via* Fenton-like reactions in acidic tumor environments to achieve CDT. Additionally, the 3-bromopyruvate can inhibit the glycolytic pathway, which results in further inhibition of tumor growth. It was found that the composite has excellent photothermal properties and a high-resolution PAI capability in NIR irradiation.

Han *et al.* explored the photoacoustic and photothermal capabilities of $Ti_3C_2T_x$ MXene by modifying it with soybean phospholipid.[70] From the *in vitro* investigations, these $Ti_3C_2T_x$ MXenes show a high photoacoustic signal intensity at an excitation wavelength of 808 nm, and the photoacoustic signal intensity increases with the increase of the composite. Moreover, when administered at a dose of 15 mg kg^{-1} in $4T_1$ tumor-bearing mice, a significant enhancement in the photoacoustic signal was observed, indicating the potential of utilizing these MXenes for PAI-guided therapy. Additionally, $Ti_3C_2T_x$ MXene has displayed excellent *in vivo* compatibility and facile elimination from the body, highlighting its potential for strong biosecurity in future clinical applications. However, MXenes face limitations as diagnostic imaging agents due to their inherent material properties. To confer specific functionality for theranostic purposes, several investigations have been conducted. One such study by Dai *et al.* involved the development of $MnO_x/Ta_4C_3T_x$ composite modified with soybean phospholipid, which acts as a contrast agent for simultaneous computed tomography (CT), tumor microenvironment-responsive T_1-weighted magnetic resonance imaging, and PAI.[90] The schematic presentation of the synthetic procedure and magnetic resonance imaging (MRI)/CT/PAI-guided photothermal cancer therapy by $MnO_x/Ta_4C_3T_x$–SP composite nanosheets are given in Fig. 6, which includes the scheme of the synthesis of $Ta_4C_3T_x$ nanosheets and $MnO_x/Ta_4C_3T_x$–SP composite nanosheets along with illustration of theranostic functions of $MnO_x/Ta_4C_3T_x$–SP. Following subcutaneous administration to mice with $4T_1$ tumors, the composite nanosheets, as made with surface modifications (SP–$MnO_x/Ta_4C_3T_x$), exhibited rapid enhancement of photoacoustic signals, with the

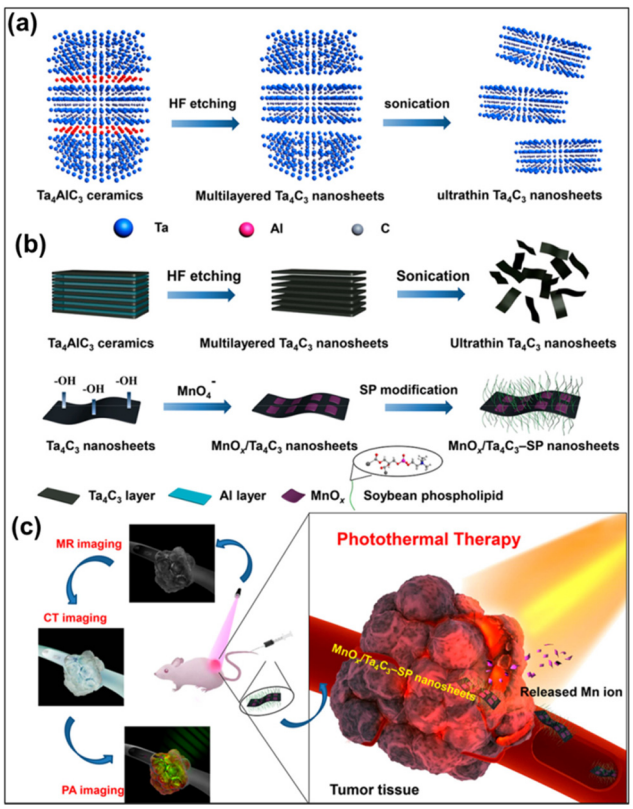

Fig. 6 Schematic presentation of the synthetic procedure and MRI/CT/PAI imaging-guided photothermal cancer therapy by $MnO_x/Ta_4C_3T_x$–SP composite nanosheets. (a) The scheme of the synthesis of 2D $Ta_4C_3T_x$ nanosheets, including HF etching, followed by sonication exfoliation. (b) The synthetic procedure for $MnO_x/Ta_4C_3T_x$–SP composite nanosheets, etching, exfoliation, *in situ* redox reaction between Ta_4C_3 nanosheets, and post-introduction of $KMnO_4$ and preceding surface SP modification. (c) Illustration of theranostic functions of $MnO_x/Ta_4C_3T_x$–SP composite nanosheets, *i.e.*, MRI/CT/PAI-guide efficient PTT tumour ablation. Reprinted with permission from ref. 90. Copyright © 2017, American Chemical Society.

maximum optical density observed at 15 min post-administration. Furthermore, the SP–MnO_x/Ta_4CT_x nanosheets demonstrated contrast-enhanced characteristics in both magnetic MRI and CT, suggesting the potential of utilizing these nanosheets for therapy guided by a variety of imaging modalities.

In another study, researchers designed 2D core–shell nanocomposites ($Ti_3C_2T_x$@Au) for applications in dual-modal imaging, specifically photoacoustic and CT.[91] The nanocomposites were synthesized using a seed-growth approach, starting from $Ti_3C_2T_x$ nanosheets. The study revealed that by coating the nanosheets with gold (Au) on their exterior, the biocompatibility and stability of the nanocomposites were significantly enhanced through thiol amendment. Moreover, the introduction of gold shell resulted in increased optical absorption in the near-infrared region. Additionally, the mild photothermal effect exerted by the nanocomposites improved tumor oxygenation and enhanced the efficacy of radiotherapy. Importantly, the nanocomposites exhibited no apparent long-term toxicity, highlighting their potential for safe biomedical applications.

Exploration of other MXenes, such as Nb_2CT_x and Mo_2CT_x for PAI was also reported. Chen *et al.* conducted a fascinating study where they successfully synthesized mesoporous-silica shells on the surface of Nb_2CT_x (Nb_2CT_x–MSN) and modified them with cetyltrimethylammonium chloride (CTAC), polyethylene glycol (PEG), and cyclic arginine–glycine–aspartic pentapeptide c(RGDyC). The synthesized composite is denoted as CTAC@Nb_2CT_x–MSN–PEG–RGD and is used for effective *in vivo* photothermal ablation of second near-infrared biowindow (NIR-II) in mouse tumor xenografts.[92] Additionally, the CTAC@Nb_2CT_x–MSN–PEG–RGD composite exhibited promising PAI capabilities. In another report, a novel therapeutic modality based on core/shell-structured Nb_2CT_x was modified with mesoporous silica (MSN) and *S*-nitrosothiol (SNO) (Nb_2CT_x–MSNs–SNO) for photonic thermogaseous therapy.[93] Here, the mesoporous silica provides the reservoirs for SNO, while the core of Nb_2CT_x creates heat shock upon NIR-II irradiation. Additionally, the Nb_2CT_x–MSNs–SNO composite can be used for PAI guidance and monitoring for precise cancer treatment. In a separate investigation, Dai *et al.* developed Mo_2CT_x MXene QDs using a straightforward liquid phase exfoliation method assisted by ultrasound.[94] The resulting Mo_2CT_x QDs demonstrated exceptional performance in PAI. Furthermore, they exhibited high biocompatibility, minimal cytotoxicity, and excellent stability, making them highly suitable for various biomedical applications. Similarly, $Ta_4C_3T_x$ modified with SP has been used for *in vivo* photoacoustic/CT dual-mode imaging combined with PTT by Lin *et al.*[95] A comparison of the recently reported MXene-based PAI systems is collectively summarized in Table 1.

4.3. Acoustic sensors

As the acoustic wave passes through or on the facet of the material, any switch to the attribute of the propagation path affects the velocity or/and amplitude of the material. These changes in the velocity can be tracked by calculating the frequency or phase features of the transducer and can be in tune with the physical quantity to be measured using acoustic sensors. Exploration of 2D materials like MOFs, transition metal oxides, transition metal dichalcogenides, *etc*. have been reported in the fabrication of acoustic sensors for a multitude of applications. Recently, MXenes have proved to be an excellent candidate for developing a variety of acoustic sensors. Compared to MXene devices, the sound-to-noise ratio (SNR) of devices based on other 2D materials falls noticeably short at the same frequencies. Additionally, the *d*-spacing between the layers of MXene measures a significant 1.31 nm, which exceeds that of other materials. These combined factors play a pivotal role in enhancing MXene's mechanical sensitivity, allowing our MXene-based acoustic sensors to demonstrate remarkable responsiveness in sensing acoustic waves across a wide audible frequency range. Researchers have recently been interested in combining macromolecules like intrinsically conducting polymers or electroactive conjugated polymers with MXenes because of their distinctive electrochemical properties, which include excellent electrical conductivity, outstanding electronic affinities, poor ionization potential, and good optical properties.[96] In a study, Derry Holaday and her coworkers reported an interesting approach of combining polyimide conducting polymer with MXene clubbed with surface acoustic waves for developing a biosensor.[97] The bioreceptor electrode was prepared by covalent immobilization of antibody of carcinoembryonic antigen (CEA) through the thioglycolic

Table 1 A comparison of the recently reported MXene-based PAI systems

MXene	Functionalization agents	Applications	Ref.
$Ti_3C_2T_x$	3-Bromopyruvate and Cu_2O	PAI-guided integrated treatment for hypoxia relief	89
$Ti_3C_2T_x$	Soybean phospholipid	PAI-guided diagnostic-imaging guidance and monitoring during therapy	70
$Ti_3C_2T_x$	Au	PAI-guided cancer imaging	91
Nb_2CT_x	CTAC, PEG, and RGDyC	*In vitro* and *in vivo* PAI	92
Nb_2CT_x	Mesoporous silica, *S*-nitrosothiol, and PEG	PAI guidance and monitoring for precise cancer treatment	93
Mo_2CT_x QDs	No modification	Photoacoustic/photothermal imaging-guided PTT for cancer	94
$Ta_4C_3T_x$	Soybean phospholipid	*In vivo* photoacoustic/CT dual-mode imaging combined with PTT	95
$Ta_4C_3T_x$	MnO_x and SP	PAI for high-performance theranostic nanoagents for efficiently combating cancer	90

acid arm linker mechanism on the delay line area of the SAW device. The biosensor was aimed to selectively detect CEA. By using a polymer-based nanocomposite system, the usual challenge of high insertion loss in polymer-based SAW analysis was effectively overcome. The excellent properties of conducting polymers, MXene, and AuNPs allows the love wave to pass through the polymer nanocomposite-coated delay line of the SAW device with minimal intensity loss. The high aspect ratio AuNPs served as active reaction sites for thioglycolic acid, promoting the formation of a dense biofilm consisting of an anti-CEA monolayer on the polyimide nanocomposite thin film, which leads to enhanced sensitivity and stability of the biosensor. The biosensor exhibited a detection limit value of 0.001 ng mL^{-1} and an upper saturation point of 120 ng mL^{-1} for CEA concentration. The biosensor exhibited excellent selectivity towards CEA and displayed minimal affinity towards common tumor markers, such as AFP (alpha-fetoprotein), cancer antigen 125, and L-tryptophan. The current biosensor's outstanding stability is another noteworthy result of the investigation. The biosensor demonstrated consistent performance for approximately 75 days without indicating a significant decline in biosensing ability.

The rapid advancement of information technology has made the field of wearable electronics diverge to a multitude of applications like health monitoring, human-skin interfacing, and electronic skin (E-skin). Flexible pressure sensors with piezoresistive, capacitive, and piezoelectric properties have been widely studied due to their easy signal acquisition, high sensitivity, simple fabrication strategy, and fast response. Ding *et al.* reported a wearable and flexible piezoresistive acoustic sensor based on MXene/poly(3,4-ethylenedioxythiophene)–poly(styrene sulfonate) (PEDOT:PSS), which was fabricated by a safe and facile drip-drying method.[98] In this sensor, PEDOT:PSS acts as a binder and connecting agent between adjacent MXene nanosheets for improving the flexibility and inherent conductivity of the MXene nanocomposite. The MXene/PEDOT:PSS acoustic sensor (MPAS) showed high sensitivity, a fast response time (57 ms), ultra-thin thickness (30 μm), and exceptional stability. The schematic representation of the detection of human physiological signals by the MPAS is given in Fig. 7. The figure shows the photograph of the acoustic sensor attached to the skin surface of the human neck and the recordings of response curves while speaking different words (Fig. 7(a–d)).

Generally, the methods for increasing the flexibility of the MXene matrix, such as flexible intercalation or the inclusion of flexible polymers, usually result in a loss in electrical characteristics. To address this issue, the conducting polymer PEDOT:PSS, which has intrinsic conductivity and flexibility, is used. Dynamic bending tests were performed to create and examine MXene/PEDOT:PSS sensing films with various mixture ratios, and the best ratio was analyzed. The sensor's superior performance allows it to detect and identify weak muscle movements and skin vibrations, such as word pronunciation. MPAS recognized sound signals with various contents, such as vowels, words, and sentences, while preserving the distinctive peaks of each audio signal. Also, this acoustic sensor introduced a novel feature in its device structure, incorporating scalable interdigital electrodes (IDE). This advancement leads to exceptional performance in detecting faint signals, such as throat articulations, skin vibration, and carotid pulse. Furthermore, when the sensor is attached to the skin surface, its capabilities are further enhanced. The carotid artery wave serves as a crucial physiological signal for detecting various aspects of cardiovascular health, including heartbeat rhythm, ejection rate, and arterial elasticity. By attaching the MPAS to the lateral surface of the human neck, it becomes possible to detect the carotid wave (Fig. 7(e) and (f)). The MPAS effectively detects and records a stable and periodic pulse signal, with each cycle represented by the green shaded curve (Fig. 7(g) and (h)). These pulse signals enable the determination of heart contraction periods and facilitate the quantitative assessment of cardiac function. As a result, the proposed MPAS holds immense value in real-time human health monitoring devices. Additionally, the MPAS was enhanced with the integration of the NR-CNN (Number Recognition Convolutional Neural Network) deep learning method, showcasing its potential in speech recognition. This novel deep learning model allows for accurate recognition of various pronunciations of frequently used numbers in everyday conversations. Remarkable results have been achieved in recognizing different number signals commonly encountered in daily interactions. The MPAS, empowered by deep learning, offers an exceptional platform for future applications in voice interaction, the advancement of artificial larynx technology, and other related fields. Notably, its outstanding performance, straightforward fabrication process, and cost-effectiveness contribute to its promising prospects.

Another interesting work by Chen *et al.* introduced a voice recognition platform based on machine learning employing a

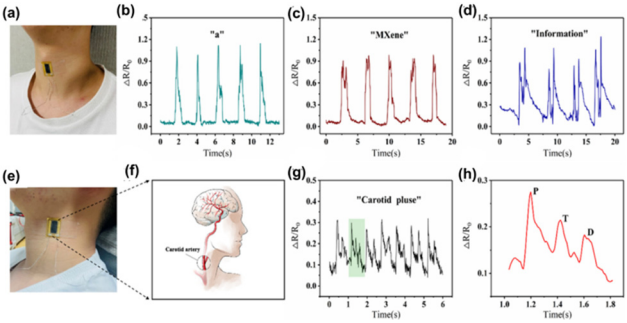

Fig. 7 Detection of human physiological signals by the MXene/PEDOT:PSS acoustic sensor (MPAS). (a) Photograph of the acoustic sensor attached to the skin surface of the human neck. (b–d) The recordings of response curves during speaking "a," "MXene," and "information," respectively. (e) Photograph of the acoustic sensor attached to the lateral surface of the human neck. (f) The location of the carotid artery in the human body. (g) Resistance changes of carotid artery pulses measured by the acoustic sensor. (h) The magnified curve of resistance changes for a single pulse time period. Reprinted with permission from ref. 98. Copyright © 2022 The Authors. Advanced Intelligent Systems published by Wiley-VCH GmbH.

very sensitive flexible vibration sensor (FVS) made of MXene/MoS_2 film.[99] A novel machine-learning-based voice analyzing platform was developed and trained to achieve high speaker recognition accuracy (99.1%) and the sensor showed a high sensitivity (25.8 mV dB^{-1}) with a broadband response of 40–3000 Hz. To fabricate the sensor patch, 0.5 mL of MXene solution was sprayed uniformly over the nitrile powder-free gloves using an airbrush, followed by spraying 0.5 mL of MoS_2 solution in a repeated manner. The bottom portion of the gloves was heated to a temperature of 70 °C and then clamped with a piece of copper strip to fabricate the sensor patch with high sensitivity. To achieve high performance, deep learning was incorporated to learn complex representations, whereas traditional algorithms that rely on hand-crafted properties were also incorporated and examined. The sensor also processed speech data-based speaker recognition using an artificial neural network (ANN) based training and testing technique. The test speaker's probability was computed in each frame, and frequency information from human sounds offered a high sensitivity.

4.4. Sonodynamic therapy

Surgical site infection (SSI) remains a major and significant postoperative complication of surgery, which can originate due to the infection occurring in the implants such as prostheses, materials, and devices. Once bacteria adhere to the surface of implants and form biofilms, prostheses loosen, pain and finally, risk of paralysis or even death for patients may happen. An estimated 160 000 to 300 000 individuals are affected by SSI every year worldwide, causing a financial cost of more than $3.5 billion. The traditional therapies against these infections are prolonged oral or intravenous antibiotics, and partial or complete explant of foreign materials may result in a severe clinical and financial burden to patients. Therefore, developing rapid, efficient, and non-invasive bacteria elimination therapies during implantation is an urgent task.

Towards this aspect, stimuli-responsive therapy can be employed by using laser irradiation, ultrasound, electricity, or magnetism to generate reactive radicals. In recent years, photo-mediated treatments have shown promising potential for similar clinical applications; however, they have some limitations, such as limited penetration depth of excitation light, inefficient delivery of the photosensitizing agents, and non-negligible peripheral tissue damage. To overcome this, sonodynamic therapy (SDT), a novel noninvasive method combining sonosensitizers and low-intensity ultrasound, can be used to eliminate the tumor or bacteria by triggering sensitive reactions to generate ROS. The schematics of the sonosensitizer-based SDT are given in Fig. 8. Compared with photo-mediated treatments, SDT possesses potentially advantageous properties of fewer side effects and deeper tissue penetration. The other advantage of this technology is the use of ultrasound that can penetrate biological tissue up to a thickness of 40 mm, almost five times that of NIR (8.5 mm). Considering that orthopaedic implants are often surrounded by soft and hard tissues, the high tissue penetration depth of ultrasound makes SDT potentially suitable for implant-related infection. MXenes exhibit the ability to quickly produce reactive oxygen species (ROS) when exposed to ultrasound, making them a highly promising choice as sonosensitizers in cancer therapy. In the evaluation of rapid ROS generation, cell penetration, and cytotoxicity in comparison to other materials, MXene stands out as an advanced material compared to other 2D materials.

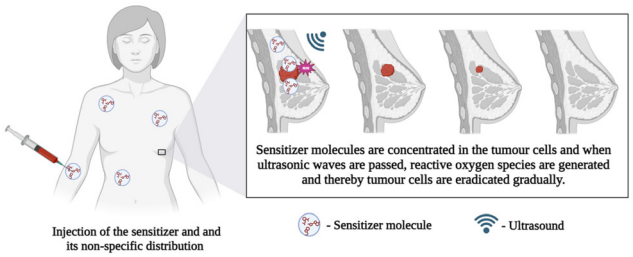

Fig. 8 Schematic representation of sonosensitizer-based sonodynamic therapy, created with BioRender.com.

Lin *et al.* developed a $Ti_3C_2T_x$ MXene-based therapeutic agent, which showed excellent absorption in the NIR II region, making it an excellent candidate for deep photothermal applications as well as photoacoustic/photothermal imaging.[100] To bestow sonodynamic functions, oxygen defect-enriched TiO_{2-x} was coated over $Ti_3C_2T_x$ by an *in situ* hydrothermal approach ($Ti_3C_2T_x$@TiO_{2-x}). When exposed to the ultrasound, $Ti_3C_2T_x$@TiO_{2-x} could generate abundant ROS due to the enhanced separation of electron–hole pairs. In another study, Chen *et al.* introduced *in situ* synthesis of nano sonosensitizers based on a $Ti_3C_2T_x$/CuO_2@bovine serum albumin (BSA) catalyst for the *in situ* generation of nanosonosensitizers by responding to the tumor microenvironment.[101] Fig. 9 shows the schematic representation of 2D MXene based *in situ* nanosonosensitizer generation for synergistic sonodynamic cancer nanotherapy including the synthetic procedure of $Ti_3C_2T_x$/CuO_2@BSA nanosheets and synergic chemodynamic and sonodynamic process. Based on a carbon matrix with a desired electrical conductivity, the CuO_2/$Ti_3C_2T_x$ sonosensitizer produced *in situ* under tumor instances improved electron and hole separation and increased SDT performance.

CaO_2-loaded $Ti_3C_2T_x$ nanosheets were used for enhanced ROS production in response to sonodynamic therapy, which can be used as an ideal antibacterial agent.[102] Here, the nanosheets exhibited chemodynamic features, which resulted in a Fenton reaction triggered by self-supplied H_2O_2. Here, the presence of CaO_2 can cause the *in situ* oxidation of $Ti_3C_2T_x$ to produce acoustic sensitizer TiO_2 on its surface. In addition, these nanosheets enabled Ca^{2+} deposition, which promoted osteogenic transformation and improved bone quality in osteomyelitis models. Wang *et al.* used a porphyrin MOF with a Schottky junction modified by $Ti_3C_2T_x$ nanosheets for SDT of osteomyelitis and bone regeneration with high efficiency.[103] Oxygen-defective $Ti_3C_2T_x$ after PEG modification and carbon dot@$Ti_3C_2T_x$ heterostructures have been used as highly efficient and safe sonosensitizers for photothermal-enhanced

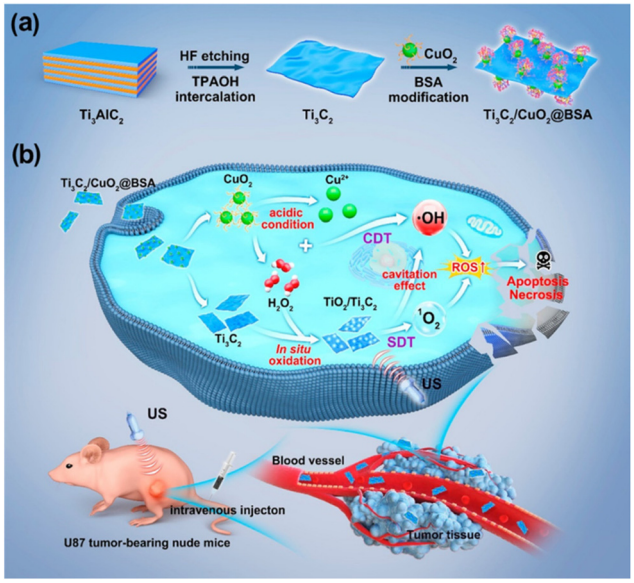

Fig. 9 Schematic representation of 2D MXene-based *in situ* nanosonosensitizer generation for synergistic sonodynamic cancer nanotherapy. (a) Schematics of the synthetic procedure of Ti_3C_2/CuO_2@BSA nanosheets. (b) Synergic chemodynamic and sonodynamic process of 2D Ti_3C_2/CuO_2@BSA nanosheets under ultrasound irradiation. Reprinted with permission from ref. 101. Copyright © 2022, American Chemical Society.

SDT of cancer.[104,105] Recently, Liu *et al.* introduced $Ti_3C_2T_x$ modified by Zn porphyrin for sonodynamic treatment of bladder cancer with the capability to remove cancer in just 15 min by the collective action of SDT and Zn^{2+}. Table 2 shows the list of reports based on the SDT application of MXenes.

Apart from $Ti_3C_2T_x$ MXene, Nb, Mo, and V-based MXenes also showed excellent sonodynamic applications for cancer therapy, antibacterial therapy as well and bone regeneration. Xu *et al.* reported the potentiality of the use of Nb_2CT_x MXene as a sonocatalytic platform in cancer therapy.[107] In this study, they used a theoretical approach for the design of MXene-based sonocatalyst and experimentally synthesized *in situ* self-oxidized Nb_2CT_x MXenes (noted as Nb_2CT_x-Ox) along with NIR-II photonic hyperthermia for tumour eradication. In another work, Yang and his coworkers reported integration of a porphyrin MOF with Nb_2CT_x as a sonosensitizer for antibacterial therapy and bone regeneration.[108] In this study, the developed sonosensitizer successfully prompted stem cell differentiation by facilitating cation transport and ATP-synthesis-linked electron transport using ultrasonic currents. In a recent study by Yu Chen *et al.*, oxygen-vacancy-rich MoO_x directly on fluorine-free Mo_2CT_x was synthesized with unique neural network-like structures.[109] These nanonetworks demonstrated excellent antibacterial efficacy, driven by their ability to capture bacteria and generate robust reactive oxygen species (ROS) when subjected to precise ultrasound irradiation. The exceptional broad-spectrum microbicidal activity of MoO_x@Mo_2CT_x nanonetworks, without harming normal tissues, was substantiated through comprehensive *in vitro* and *in vivo* assessments. Xiaogang Qu and his colleagues used V_2CT_x MXene quantum dots through an Nrf2 antioxidant mechanism, and ultrasound-assisted ROS generation served as one of the best anticancer nanoagents. The quantum dots also decreased the expression of associated downstream antioxidant enzymes, increasing the cytotoxicity of ROS during SDT.[110] These above examples showed the efficacy of MXenes as one of the best materials for use as a sonosensitizer for SDT in tumor therapy.

4.5. Thermoacoustic device

The generation of sound sources from different types of energy, such as electrical energy, mechanical energy, light energy (optoacoustics), and water (underwater acoustics) are

Table 2 Various reports of SDT application of different MXenes

Material	Technique	Mechanism	Application	Ref.
CaO_2–TiO_x@$Ti_3C_2T_x$	Sonodynamic therapy	ROS generation	Antibacterial activity, bone tissue regeneration	102
Porphyrin MOF-$Ti_3C_2T_x$	Sonodynamic therapy	ROS generation	Osteomyelitis, bone regeneration	103
Oxygen-defective $Ti_3C_2T_x$–PEG nanosheets	Photothermal therapy enhanced sonodynamic therapy	ROS generation	Cancer therapy	104
Carbon dot@$Ti_3C_2T_x$	Mild photothermal therapy-enhanced SDT	ROS generation	Tumour therapy	105
Ti_3C_2/CuO_2@BSA	Sonodynamic nanotherapy	Oxidative phosphorylation, ROS generation apoptosis	Tumour therapy	101
$Ti_3C_2T_x$/ZnTCPP	Sonodynamic therapy	ROS generation	Bladder cancer therapy	106
$Ti_3C_2T_x$@TiO_{2-x}	NIR-II photothermal enhanced Sonodynamic therapy	ROS generation	Antitumour therapy	100
Nb_2CT_x-Ox	NIR-II photothermal hyperthermia and sonodynamic therapy	ROS generation	Tumour therapy	107
Porphyrin MOF-Nb_2CT_x	Sonodynamic therapy	ATP synthesis, ROS generation	Antibacterial therapy and bone regeneration	108
MoO_x@Mo_2CT_x	Sonocatalytic therapy	ROS generation	Bacterial eradication	109
V_2CT_x quantum dots	Nrf2 antioxidant mechanism, sonodynamic therapy	ROS generation	Cancer therapy	110

reported in the literature. The conversion of heat energy to acoustic energy, denoted as thermoacoustic, is an advancement in this field. The possibility of thin films and membranes converting energy from one medium to sound energy, especially using 2D materials like graphene,[111] transition metal oxide,[112] and 1D materials like carbon nanotubes,[113] and nanowires[73,114] have been used conventionally in the past decades. Usually, there will be a substrate on which a layer of conducting material is coated, and driving energy will be passed to these layers and it will pass to the air molecules, thereby causing a temperature rise. This temperature rise, *i.e.*, heat energy, produces sound energy, the basic mechanism behind the thermoacoustic effect which is explained in Fig. 10.

The interlayer distance between the MXene layers is 1.31 nm, which is about 3 times greater than that of graphene (0.335 nm) and other 2D materials. Therefore, it can offer an ultrasmall heat capacity per unit area (HCPUA) and promote enhancement in the efficiency of heat transfer into the surrounding air medium. Consequently, it becomes feasible to construct a sound source device that leverages the thermoacoustic effect, employing an ultrathin MXene film. In a recent study by Gou *et al.*, the possibility of using MXenes as a thermoacoustic sound source has been explored.[115] The important requirement that needs to be met by a high-performance sound source is a lower value of minimal heat capacity per unit area (HCPUA). A thin MXene film with a low HCPUA and unique layered structure is considered an emerging possible option to be used in making acoustic devices. The second requirement for a high-performance sound source is that the thermal conductivity of the substrate must be low enough, or the conductive film must be suspended as far from the substrate as feasible to prevent heat loss from the substrate. Towards this aspect, they have successfully made sound source devices on anodic aluminium oxide (AAO) and flexible polyimide (PI) substrates using the synthesized $Ti_3C_2T_x$ nanoflakes. The AAO substrate contains numerous holes, which can lower thermal leakage from the substrate and increase heat transfer effectiveness. The basic mechanism involved in sound generation is that a tiny layer of air molecules on the film surface can be heated up when AC voltage is given to the MXene device, causing the MXene film to produce Joule heating, which causes the periodicity of the air vibration to produce sound waves. The dynamic frequency analyzer and the conventional microphone, respectively, receive and analyze the sound waves at this point. With a frequency range of 100 Hz to 20 kHz, the as-developed MXene sound source device on an AAO substrate demonstrated a higher SPL of 68.2 dB (f = 15 kHz) and a relatively steady sound spectrum output. Moreover, a flexible PI substrate-based MXene sound source device has also been mounted to the fingers, back of the hand, and arms, exhibiting its outstanding acoustic wearability, as shown in Fig. 11. The schematic representation of the device and the sound pressure level response of the device at different powers and under different radii of curvature are given in Fig. 11(a–c). The flexible device attached to an arm, the backside of the palm, and the finger, with their sound pressure level response, are given in Fig. 11(d–f), respectively. The sound pressure level response of the flexible device is attached to an arm, backside of the palm, and finger, respectively. In addition, they have also made flexible MXene earphones and evaluated the sound pressure level response compared with those of commercial earphones.

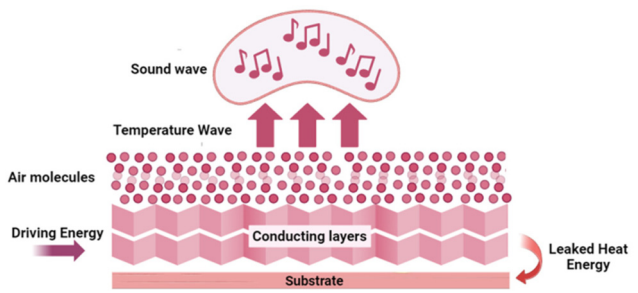

Fig. 10 Working principle of a thermoacoustic sound source, created with BioRender.com.

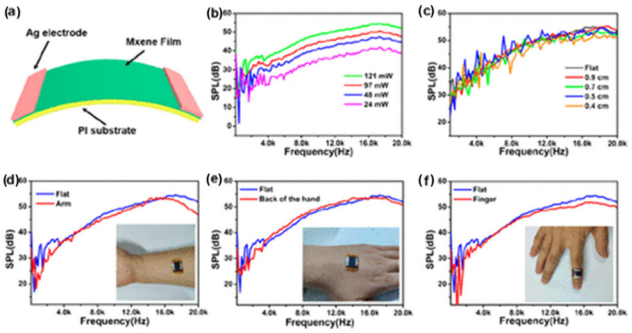

Fig. 11 Performance of the flexible MXene-based acoustic device on the PI substrate. (a) Schematic representation of the device. (b) The sound pressure level response of the PI-based MXene device at different powers. (c) The sound pressure level response of the MXene device under different radii of curvature. (d–f) The sound pressure level response of the flexible device attached to an arm, backside of the palm, and finger, respectively. Reprinted with permission from ref. 115. Copyright © 2019, American Chemical Society.

5. Challenges and future prospects

MXenes have emerged as an expanding research domain, exhibiting significant growth over the past decade, as evidenced by the extensive literature in the field. The incorporation of acoustic platforms into the realm of MXenes has unveiled a fresh dimension in biomedical research. The remarkable electronic, mechanical, and biological characteristics inherent to MXenes underlay these notable advancements.[116] Based on this comprehensive review, it is apparent that the utilization of MXenes in acoustic platforms holds promise for applications such as cancer therapeutics and the development of acoustic sensors. Artificial eardrums and sound detectors constructed with MXene materials exhibit a remarkable combination of flexi-

bility and lightweight attributes in contrast to their conventional rigid and bulky counterparts. This breakthrough paves the way for innovative wearable devices, particularly those focused on enhancing human–machine interaction.[117] Furthermore, the biocompatibility of MXenes has found diverse applications, including their utilization as sonosensitizers in cancer therapies like sonodynamic therapy. Additionally, these materials have been harnessed as imaging agents in the realm of PAI, further showcasing their versatility and potential in biomedical contexts.

While the potential of MXene-based acoustics applications is evident, several technical challenges must be addressed for successful real-world implementation. Among these challenges, the chemical instability of most MXenes is an important point to consider. The instability is characterized by issues such as oxidation, restacking, colloidal solution instability, swelling, and thin film degradation, which hampers their catalytic, storage, and electron shielding capabilities, thereby significantly constraining their widespread research and industrial applications. Consequently, addressing this challenge has become an important research topic among researchers. To enhance the stability of MXenes, various strategies are being explored, including optimizing the synthesis of MAX phases, modifying MXene preparation techniques (*e.g.*, promoting ordered assembly and modifying terminations),[118] and controlling storage conditions (*e.g.*, frozen storage under an inert gas atmosphere).[119] Other methods include implementing protective measures such as functionalization[120,121] or surface modification by introducing appropriate antioxidants,[122] silane coupling agents,[123] and biopolymers[124] at the surface and edges of MXene flakes.

Another prominent challenge is achieving optimal conductivity in acoustic devices such as voice recognition tools and artificial eardrums. Conventionally, fabricating these devices has relied on methods like vacuum filtration, dip-coating, inkjet coating, spray coating, and chemical vapor deposition (CVD) over the past decades. However, processes like CVD can damage the nanomaterial and thereby diminish its properties, and most importantly, these techniques are expensive. While coating techniques can overcome those challenges, the conductivity of the material remains a big question mark. To overcome these hurdles, it becomes imperative to explore innovative fabrication techniques like 3D printing, 3D bioprinting, *etc*. By embracing such approaches, the development of novel devices could hold the key to surmounting existing limitations and unlocking the full potential of MXene-based acoustics in various applications.

Another challenge we face is the interaction between human skin and machine surface. When we broadly analyze the challenges of acoustic devices-based wearable systems, the human skin, sensor, and material interface are the most discussed challenges. Our human skin is soft, stretchable, and has an outer viscoelastic epidermal layer with a unique surface contour that acts as a barrier for the exchange of fluids. The wearability is fundamentally decided by the materials that align with the epidermal layer's physical, chemical, and biological aspects. Skin irritation and discomfort are caused by entering foreign materials, demanding the skin material interface to consider all these prerequisites. The contact of the skin surface with these devices can cause irritations and allergies. Acoustic devices are still in their blooming stage with many upgrades in performance (accuracy, resolution, detection limit, reliability, durability) and the analyzing parameters (temperature, hydration, pressure). The individual factors that act as a barrier have to be improved with new materials like MXenes. Furthermore, the optimization of transduction mechanisms within acoustic devices could be enhanced through the incorporation of the triboelectric effect.[125] When acoustic devices are attached to the skin surface, the skin friction and the interaction of skin with the machine studies, *i.e.*, skin tribology, have to be addressed.[126] In the design of artificial eardrums, the interaction of the tympanic membrane (middle ear) with the device must also be studied.

In PAI, to learn more about the cytotoxicity impacts and long-term stability of MXenes under *in vivo* environments, similar techniques may be used to investigate the interaction of MXenes with biomolecules.[127] To realize the promise of MXenes for biological applications, storage technology for effective storage and improvements in thermal and oxidative stability must be addressed. Simulation studies may prove to be a beneficial tool in this regard. Moreover, the fusion of wearable technology, the Internet of Things (IoT), and artificial intelligence (AI) with acoustic sensors holds promise for charting new trajectories.[128–130] The acoustic detection of biomarkers, environmental contaminants, *etc*., can be expected in the coming years with advanced technologies.

Other acoustic techniques like acoustic tweezers,[97] acoustic levitation,[131] acoustic separation,[132] surface acoustic wave sensors,[133] *etc*., are explored with other nanomaterials, but exploration with MXenes is still in the blooming stage. Also, the integration of acoustics with microfluidics, *i.e.*, acoustofluidics, is explored only in the synthesis of MXenes, but the application window, like acoustofluidic diagnosis, is not explored. There are also other fluidic techniques like nanofluidics, optofluidics, angstrom fluidics, *etc*. with which acoustics can be integrated and can be presented as a realm of exploration.[134–136]

In the context of thermoacoustic application, MXenes were only used to produce sound and fabrication of acoustic devices. The possibility of microwave-induced thermoacoustic imaging can be explored for cancer therapy when combined with microwave technology.[137] Since MXenes are good microwave absorbers, they act as information carriers and pass to form ultrasound energy transfer and they can achieve non-destructive, high-resolution imaging of deep cells and tissues.[138] Therefore, MXene-based microwave-induced thermoacoustic imaging of cell-related studies can be expected shortly. Non-thermal acoustic treatment using MXenes can be regarded as a safe alternative protocol to thermosensitive hyperthermia for cancer therapy, and more studies have to be done. Overcoming challenges and exploring future prospects in MXene acoustics can open new directions in the palette of biomedical applications. Fig. 12 shows the schematic represen-

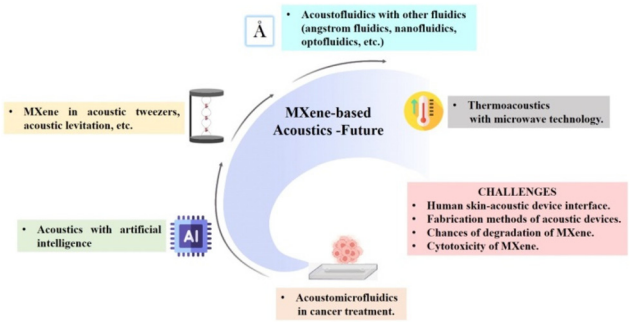

Fig. 12 Schematic representation of the future perspectives and the major challenges of MXene-based acoustics platforms, created with BioRender.com.

tation of the future perspectives and the major challenges on MXene-based acoustics platforms. This includes the expected future applications of MXenes in acoustic tweezers, thermoacoustics, acoustofluidics, acoustomicrofluidics, AI-enabled acoustics, *etc*. The major challenges faced in the previous studies include degradation and cytotoxicity of MXene, fabrication methods of the acoustic device, and human skin–acoustic device interface.

6. Conclusions

The focal point of this review predominantly illustrated the utilization of MXenes within the domain of acoustics. The scope of the article encompassed a broad spectrum, spanning from the acoustic synthesis of MXenes to diverse applications such as developing artificial eardrums, facilitating PAI, fabricating acoustic sensors, engineering thermoacoustic devices, and advancing sonodynamic therapy. Exciting prospects are arising in the medical realm with the utilization of acoustics technology. This innovation offers patients not only pain-free and side-effect-free treatments but also enhanced outcomes, serving as a foundation for the advancement of smart and digital healthcare in the future. The potential integration of MXene nanomaterials into medical applications holds the promise of paving a path for their substantial role in the times ahead. Despite significant challenges, our conviction remains that the progress in nanomaterials and nanotechnologies can drive the achievements of acoustic devices in the forthcoming years.

Author contributions

The manuscript was written through the contributions of all authors. All authors have given approval to the final version of the manuscript.

Conflicts of interest

The authors declare no conflicts of interests.

Acknowledgements

PAR acknowledges Ramalingaswami Re-entry fellowship (BT/RLF/Re-entry/75/2020) from the Department of Biotechnology (DBT), Govt. of India. The authors thank Indian Institute of Technology Palakkad and Bharathiar University for the constant support.

References

1 C. Dal Lin, C. M. Radu, G. Vitiello, P. Romano, A. Polcari, S. Iliceto, P. Simioni and F. Tona, *Int. J. Mol. Sci.*, 2021, **22**, 156.
2 T. G. Leighton, *Prog. Biophys. Mol. Biol.*, 2007, **93**, 3–83.
3 C. J. Harvey, J. M. Pilcher, R. J. Eckersley, M. J. K. Blomley and D. O. Cosgrove, *Clin. Radiol.*, 2002, **57**, 157–177.
4 M. Shin, S. Q. Lee, F. M. Fazi, P. A. Nelson, D. Kim, S. Wang, K. H. Park and J. Seo, *J. Acoust. Soc. Am.*, 2010, **128**, 121–131.
5 V. Ciaravino, *Med. Phys.*, 1986, **13**, 424–424.
6 E. Bercovich and M. C. Javitt, *Rambam Maimonides Med. J.*, 2018, **9**, e0034.
7 A. Z. Alkilani, M. T. McCrudden and R. F. Donnelly, *Pharmaceutics*, 2015, **7**, 438–470.
8 Y. Zhuang, J. Li, Q. Hu, S. Han, W. Liu, C. Peng, Z. Li, L. Zhang, X. Wei and Z. Xu, *Compos. Sci. Technol.*, 2020, **200**, 108386.
9 L. E. Derchi, G. Serafini, N. Gandolfo, N. G. Gandolfo and C. Martinoli, *Eur. Radiol.*, 2001, **11**, 2137–2155.
10 C. Jenssen and C. F. Dietrich, *Best Pract. Res., Clin. Gastroenterol.*, 2009, **23**, 743–759.
11 M. Prasad, V. Sahula and V. K. Khanna, *IEEE Trans. Semicond. Manuf.*, 2013, **26**, 233–241.
12 R. Rasouli, K. M. Villegas and M. Tabrizian, *Lab Chip*, 2023, **23**, 1300–1338.
13 D. Wu, D. Baresch, C. Cook, Z. Ma, M. Duan, D. Malounda, D. Maresca, M. P. Abundo, J. Lee, S. Shivaei, D. R. Mittelstein, T. Qiu, P. Fischer and M. G. Shapiro, *Sci. Adv.*, 2023, **9**, eadd9186.
14 R. Ahmad, G. Destgeer, M. Afzal, J. Park, H. Ahmed, J. H. Jung, K. Park, T.-S. Yoon and H. J. Sung, *Anal. Chem.*, 2017, **89**, 13313–13319.
15 S. Santesson and S. Nilsson, *Anal. Bioanal. Chem.*, 2004, **378**, 1704–1709.
16 M. Kaynak, P. Dirix and M. S. Sakar, *Adv. Sci.*, 2020, **7**, 2001120.
17 F. Petersson, L. Åberg, A.-M. Swärd-Nilsson and T. Laurell, *Anal. Chem.*, 2007, **79**, 5117–5123.
18 D. J. Collins, C. Devendran, Z. Ma, J. W. Ng, A. Neild and Y. Ai, *Sci. Adv.*, 2016, **2**, e1600089.
19 J. Rufo, F. Cai, J. Friend, M. Wiklund and T. J. Huang, *Nat. Rev. Methods Primers*, 2022, **2**, 30.
20 C. Peng, M. Chen, J. B. Spicer and X. Jiang, *Sens. Actuators, A*, 2021, **332**, 112719.

21 C. H. Zhang, Z. Hu, G. Gao, S. Zhao and Y. D. Huang, *Mater. Des.*, 2013, **46**, 503–510.
22 C. Caneva, I. M. De Rosa and F. Sarasini, *Strain*, 2008, **44**, 308–316.
23 A. Pal and N. Chauhan, *J. Mol. Liq.*, 2009, **149**, 29–36.
24 C. M. Flannery and H. von Kiedrowski, *Ultrasonics*, 2002, **40**, 83–87.
25 T. Kim, Q. Zhang, J. Li, L. Zhang and J. V. Jokerst, *ACS Nano*, 2018, **12**, 5615–5625.
26 Y. Chen, X. Ding, S.-C. Steven Lin, S. Yang, P.-H. Huang, N. Nama, Y. Zhao, A. A. Nawaz, F. Guo, W. Wang, Y. Gu, T. E. Mallouk and T. J. Huang, *ACS Nano*, 2013, **7**, 3306–3314.
27 J. Zhang, Y. Li, S. Cheng, J. Zhou, S. Wang, D. Zhao, C. Shi, F. Ma, X. Chen and J. Shao, *ACS Appl. Nano Mater.*, 2022, **5**, 14654–14662.
28 N. Rohaizad, C. C. Mayorga-Martinez, M. Fojtů, N. M. Latiff and M. Pumera, *Chem. Soc. Rev.*, 2021, **50**, 619–657.
29 F. R. Fan, R. Wang, H. Zhang and W. Wu, *Chem. Soc. Rev.*, 2021, **50**, 10983–11031.
30 A. Garg, S. Basu, N. P. Shetti and K. R. Reddy, *J. Environ. Chem. Eng.*, 2021, **9**, 106408.
31 W. Ni, P. Lu, X. Fu, W. Zhang, P. P. Shum, H. Sun, C. Yang, D. Liu and J. Zhang, *Opt. Express*, 2018, **26**, 20758–20767.
32 J. Li, Z. Liao, T. Liang, S. Zhang, B. Tang, X. Fu, G. Li and Y. Huang, *Comput. Electron. Agric.*, 2022, **200**, 107267.
33 D. Matatagui, O. Kolokoltsev, J. M. Saniger, I. Gràcia, M. J. Fernández, J. L. Fontecha and M. del Carmen Horrillo, *Sensors*, 2017, **17**, 2624.
34 D. Scolfaro, M. Finamor, L. O. Trinchão, B. L. T. Rosa, A. Chaves, P. V. Santos, F. Iikawa and O. D. D. Couto, Jr., *ACS Nano*, 2021, **15**, 15371–15380.
35 J. Devkota, K.-J. Kim, P. R. Ohodnicki, J. T. Culp, D. W. Greve and J. W. Lekse, *Nanoscale*, 2018, **10**, 8075–8087.
36 A. M. Evans, N. P. Bradshaw, B. Litchfield, M. J. Strauss, B. Seckman, M. R. Ryder, I. Castano, C. Gilmore, N. C. Gianneschi, C. R. Mulzer, M. C. Hersam and W. R. Dichtel, *Adv. Mater.*, 2020, **32**, 2004205.
37 F. Iikawa, A. Hernández-Mínguez, I. Aharonovich, S. Nakhaie, Y.-T. Liou, J. M. J. Lopes and P. V. Santos, *Appl. Phys. Lett.*, 2019, **114**, 171104.
38 W. Zhang, Z. Shen, Y. Wu, W. Zhang, T. Zhang, B.-Y. Yu, X. Zheng and J. Tian, *Anal. Chim. Acta*, 2022, **1204**, 339737.
39 G.-Y. Gou, X.-S. Li, J.-M. Jian, H. Tian, F. Wu, J. Ren, X.-S. Geng, J.-D. Xu, Y.-C. Qiao, Z.-Y. Yan, G. Dun, C. W. Ahn, Y. Yang and T.-L. Ren, *Sci. Adv.*, 2022, **8**, eabn2156.
40 A. Khunger, N. Kaur, Y. K. Mishra, G. Ram Chaudhary and A. Kaushik, *Mater. Lett.*, 2021, **304**, 130656.
41 J. Huang, Z. Li, Y. Mao and Z. Li, *Nano Sel.*, 2021, **2**, 1480–1508.
42 L. Damptey, B. N. Jaato, C. S. Ribeiro, S. Varagnolo, N. P. Power, V. Selvaraj, D. Dodoo-Arhin, R. V. Kumar, S. P. Sreenilayam, D. Brabazon, V. Kumar Thakur and S. Krishnamurthy, *Global Challenges*, 2022, **6**, 2100120.
43 S. Iravani and R. S. Varma, *ACS Biomater. Sci. Eng.*, 2021, **7**, 1900–1913.
44 B. Richard, S. A. Thomas, A. Reddy M., M. R. Pallavolu and J. Cherusseri, *Energy Fuels*, 2023, **37**, 6999–7013.
45 M. Han, C. E. Shuck, R. Rakhmanov, D. Parchment, B. Anasori, C. M. Koo, G. Friedman and Y. Gogotsi, *ACS Nano*, 2020, **14**, 5008–5016.
46 W. Huang, L. Hu, Y. Tang, Z. Xie and H. Zhang, *Adv. Funct. Mater.*, 2020, **30**, 2005223.
47 P. A. Rasheed, R. P. Pandey, F. Banat and S. W. Hasan, *Matter*, 2022, **5**, 546–572.
48 Y. Gogotsi and B. Anasori, *ACS Nano*, 2019, **13**, 8491–8494.
49 A. Bhat, S. Anwer, K. S. Bhat, M. I. H. Mohideen, K. Liao and A. Qurashi, *npj 2D Mater. Appl.*, 2021, **5**, 61.
50 B. Anasori, M. R. Lukatskaya and Y. Gogotsi, *Nat. Rev. Mater.*, 2017, **2**, 16098.
51 K. Rasool, R. P. Pandey, P. A. Rasheed, S. Buczek, Y. Gogotsi and K. A. Mahmoud, *Mater. Today*, 2019, **30**, 80–102.
52 M. Han, Y. Liu, R. Rakhmanov, C. Israel, M. A. S. Tajin, G. Friedman, V. Volman, A. Hoorfar, K. R. Dandekar and Y. Gogotsi, *Adv. Mater.*, 2021, **33**, 2003225.
53 S. Bai, M. Yang, J. Jiang, X. He, J. Zou, Z. Xiong, G. Liao and S. Liu, *npj 2D Mater. Appl.*, 2021, **5**, 78.
54 M. Ankitha, N. Shabana, A. M. Arjun and P. A. Rasheed, *Carbon Trends*, 2022, **9**, 100232.
55 L. Zhao, L. Wang, Y. Zheng, S. Zhao, W. Wei, D. Zhang, X. Fu, K. Jiang, G. Shen and W. Han, *Nano Energy*, 2021, **84**, 105921.
56 Y. Huang, Q. Lu, D. Wu, Y. Jiang, Z. Liu, B. Chen, M. Zhu and O. G. Schmidt, *Carbon Energy*, 2022, **4**, 598–620.
57 V. Soni, P. Singh, H. H. Phan Quang, A. A. Parwaz Khan, A. Bajpai, Q. Van Le, V. K. Thakur, S. Thakur, V.-H. Nguyen and P. Raizada, *Chemosphere*, 2022, **293**, 133541.
58 P. J. Jandas, K. Prabakaran, J. Luo, C. Fu, Y. Q. Fu and M. G. Derry Holaday, *Sens. Actuators, A*, 2021, **331**, 112998.
59 Y. Wang and Y. Wang, *SmartMat*, 2023, **4**, e1130.
60 R. Deng, M. Chang, Y. Chen and Y. Zhou, *Nanophotonics*, 2022, **11**, 4995–5017.
61 C. Peng, P. Wei, X. Chen, Y. Zhang, F. Zhu, Y. Cao, H. Wang, H. Yu and F. Peng, *Ceram. Int.*, 2018, **44**, 18886–18893.
62 K.-Y. Sun, Y. Wu, J. Xu, W. Xiong, W. Xu, J. Li, Z. Sun, Z. Lv, X. S. Wu, Q. Jiang, H.-L. Cai and D. Shi, *Bioact. Mater.*, 2022, **8**, 435–448.
63 B. Shen, X. Liao, X. Zhang, H.-T. Ren, J.-H. Lin, C.-W. Lou and T.-T. Li, *Electrochim. Acta*, 2022, **413**, 140144.
64 M. Song, S.-Y. Pang, F. Guo, M.-C. Wong and J. Hao, *Adv. Sci.*, 2020, **7**, 2001546.
65 Y.-J. Kim, S. J. Kim, D. Seo, Y. Chae, M. Anayee, Y. Lee, Y. Gogotsi, C. W. Ahn and H.-T. Jung, *Chem. Mater.*, 2021, **33**, 6346–6355.
66 M. Naguib, R. R. Unocic, B. L. Armstrong and J. Nanda, *Dalton Trans.*, 2015, **44**, 9353–9358.

67 G. P. Neupane, B. Wang, M. Tebyetekerwa, H. T. Nguyen, M. Taheri, B. Liu, M. Nauman and R. Basnet, *Small*, 2021, **17**, 2006309.
68 H. Alijani, A. R. Rezk, M. M. Khosravi Farsani, H. Ahmed, J. Halim, P. Reineck, B. J. Murdoch, A. El-Ghazaly, J. Rosen and L. Y. Yeo, *ACS Nano*, 2021, **15**, 12099–12108.
69 A. E. Ghazaly, H. Ahmed, A. R. Rezk, J. Halim, P. O. Persson, L. Y. Yeo and J. Rosen, *ACS Nano*, 2021, **15**, 4287–4293.
70 X. Han, J. Huang, H. Lin, Z. Wang, P. Li and Y. Chen, *Adv. Healthcare Mater.*, 2018, **7**, 1701394.
71 C. Peng, M. Chen, J. B. Spicer and X. Jiang, *Sens. Actuators, A*, 2021, **332**, 112719.
72 H. Sun, X. Gao, L.-Y. Guo, L.-Q. Tao, Z. H. Guo, Y. Shao, T. Cui, Y. Yang, X. Pu and T.-L. Ren, *InfoMat*, 2023, **5**, e12385.
73 Y. Jin, B. Wen, Z. Gu, X. Jiang, X. Shu, Z. Zeng, Y. Zhang, Z. Guo, Y. Chen, T. Zheng, Y. Yue, H. Zhang and H. Ding, *Adv. Mater. Technol.*, 2020, **5**, 2000262.
74 L. Lin and L. V. Wang, *Nat. Rev. Clin. Oncol.*, 2022, **19**, 365–384.
75 Y. Tian, H. Tian, Y. L. Wu, L. L. Zhu, L. Q. Tao, W. Zhang, Y. Shu, D. Xie, Y. Yang, Z. Y. Wei, X. H. Lu, T.-L. Ren, C.-K. Shih and J. Zhao, *Sci. Rep.*, 2015, **5**, 10582.
76 Y. Du, Q. Jiang, N. Beziere, L. Song, Q. Zhang, D. Peng, C. Chi, X. Yang, H. Guo, G. Diot, V. Ntziachristos, B. Ding and J. Tian, *Adv. Mater.*, 2016, **28**, 10000–10007.
77 X. Liu, Y. Duan, D. Hu, M. Wu, C. Chen, P. B. Ghode, G. Magarajah, N. Thakor, X. Liu, C. Liu, Z. Sheng, H. Zheng and B. Liu, *ACS Mater. Lett.*, 2021, **3**, 1284–1290.
78 J. Lavaud, M. Henry, J. L. Coll and V. Josserand, *Int. J. Pharm.*, 2017, **532**, 704–709.
79 A. Liopo, R. Su and A. A. Oraevsky, *Photoacoustics*, 2015, **3**, 35–43.
80 A. Krumholz, D. M. Shcherbakova, J. Xia, L. V. Wang and V. V. Verkhusha, *Sci. Rep.*, 2014, **4**, 3939.
81 J. Weber, P. C. Beard and S. E. Bohndiek, *Nat. Methods*, 2016, **13**, 639–650.
82 S. Zanganeh, H. Li, P. Kumavor, U. Alqasemi, A. Aguirre, I. Mohammad, C. Stanford, M. Smith and Q. Zhu, *J. Biomed. Opt.*, 2013, **18**, 096006.
83 M. Hajfathalian, A. Amirshaghaghi, P. C. Naha, P. Chhour, J. C. Hsu, K. Douglas, Y. Dong, C. M. Sehgal, A. Tsourkas, S. Neretina and D. P. Cormode, *Nanoscale*, 2018, **10**, 18749–18757.
84 M. A. Patel, H. Yang, P. L. Chiu, D. D. T. Mastrogiovanni, C. R. Flach, K. Savaram, L. Gomez, A. Hemnarine, R. Mendelsohn, E. Garfunkel, H. Jiang and H. He, *ACS Nano*, 2013, **7**, 8147–8157.
85 A. de la Zerda, Z. Liu, S. Bodapati, R. Teed, S. Vaithilingam, B. T. Khuri-Yakub, X. Chen, H. Dai and S. S. Gambhir, *Nano Lett.*, 2010, **10**, 2168–2172.
86 Z. Chaudhary, G. M. Khan, M. M. Abeer, N. Pujara, B. Wan-Chi Tse, M. A. McGuckin, A. Popat and T. Kumeria, *Biomater. Sci.*, 2019, **7**, 5002–5015.
87 W. Zhu, M. Chen, Y. Liu, Y. Tian, Z. Song, G. Song and X. Zhang, *Nanoscale*, 2019, **11**, 20630–20637.
88 D. Wang, Z. Zhang, L. Lin, F. Liu, Y. Wang, Z. Guo, Y. Li, H. Tian and X. Chen, *Biomaterials*, 2019, **223**, 119459.
89 Z. Wang, H. Li, W. She, X. Zhang, Y. Liu, Y. Liu and P. Jiang, *Anal. Chem.*, 2023, **95**, 1710–1720.
90 C. Dai, Y. Chen, X. Jing, L. Xiang, D. Yang, H. Lin, Z. Liu, X. Han and R. Wu, *ACS Nano*, 2017, **11**, 12696–12712.
91 W. Tang, Z. Dong, R. Zhang, X. Yi, K. Yang, M. Jin, C. Yuan, Z. Xiao, Z. Liu and L. Cheng, *ACS Nano*, 2019, **13**, 284–294.
92 X. Han, X. Jing, D. Yang, H. Lin, Z. Wang, H. Ran, P. Li and Y. Chen, *Theranostics*, 2018, **8**, 4491–4508.
93 H. Yin, X. Guan, H. Lin, Y. Pu, Y. Fang, W. Yue, B. Zhou, Q. Wang, Y. Chen and H. Xu, *Adv. Sci.*, 2020, **7**, 1901954.
94 W. Dai, H. Dong and X. Zhang, *Materials*, 2018, **11**, 1776.
95 H. Lin, Y. Wang, S. Gao, Y. Chen and J. Shi, *Adv. Mater.*, 2018, **30**, 1703284.
96 W. Luo, Y. Ma, T. Li, H. K. Thabet, C. Hou, M. M. Ibrahim, S. M. El-Bahy, B. B. Xu and Z. Guo, *J. Energy Storage*, 2022, **52**, 105008.
97 P. Jandas, K. Prabakaran, J. Luo, C. Fu, Y. Q. Fu and M. G. Derry Holaday, *Sens. Actuators, A*, 2021, **331**, 112998.
98 H. Ding, Z. Zeng, Z. Wang, X. Li, T. Yildirim, Q. Xie, H. Zhang, S. Wageh, A. A. Al-Ghamdi, X. Zhang and B. Wen, *Adv. Intell. Syst.*, 2022, **4**, 2200140.
99 J. Chen, L. Li, W. Ran, D. Chen, L. Wang and G. Shen, *Nano Res.*, 2023, **16**, 3180–3187.
100 D.-Y. Zhang, H. Liu, M. R. Younis, S. Lei, Y. Chen, P. Huang and J. Lin, *J. Nanobiotechnol.*, 2022, **20**, 53.
101 M. Zhang, D. Yang, C. Dong, H. Huang, G. Feng, Q. Chen, Y. Zheng, H. Tang, Y. Chen and X. Jing, *ACS Nano*, 2022, **16**, 9938–9952.
102 Y. Yu, H. Sun, Q. Lu, J. Sun, P. Zhang, L. Zeng, K. Vasilev, Y. Zhao, Y. Chen and P. Liu, *J. Nanobiotechnol.*, 2023, **21**, 193.
103 H. Wang, N. Mu, Y. He, X. Zhang, J. Lei, C. Yang, L. Ma and Y. Gao, *Theranostics*, 2023, **13**, 1669–1683.
104 G. Li, X. Zhong, X. Wang, F. Gong, H. Lei, Y. Zhou, C. Li, Z. Xiao, G. Ren, L. Zhang, Z. Dong, Z. Liu and L. Cheng, *Bioact. Mater.*, 2022, **8**, 409–419.
105 B. Geng, S. Xu, L. Shen, F. Fang, W. Shi and D. Pan, *Carbon*, 2021, **179**, 493–504.
106 H. Liu, T. Xing, W. Wang and H. Hao, *Mater. Lett.*, 2023, **350**, 134983.
107 J. Xu, L. Chen, S. Ding, X. Dai, Y. Dai, Y. Chen and X. Ni, *Nano Today*, 2023, **48**, 101750.
108 L. Ma, X. Zhang, H. Wang, X. Feng, J. Lei, Y. He, J. Wei, Y. Zhang, L. Tan and C. Yang, *Sci. China Mater.*, 2023, **66**, 2913–2924.
109 L. Zong, Y. Yu, J. Wang, P. Liu, W. Feng, X. Dai, L. Chen, C. Gunawan, S. L. Jimmy Yun, R. Amal, S. Cheong, Z. Gu and Y. Chen, *Biomaterials*, 2023, **296**, 122074.
110 H. Wang, X. Liu, X. Yan, J. Fan, D. Li, J. Ren and X. Qu, *Chem. Sci.*, 2022, **13**, 6704–6714.
111 J. W. Suk, K. Kirk, Y. Hao, N. A. Hall and R. S. Ruoff, *Adv. Mater.*, 2012, **24**, 6342–6347.

112 H. Tian, D. Xie, Y. Yang, T.-L. Ren, Y.-F. Wang, C.-J. Zhou, P.-G. Peng, L.-G. Wang and L.-T. Liu, *Appl. Phys. Lett.*, 2011, **99**, 043503.
113 B. J. Mason, S.-W. Chang, J. Chen, S. B. Cronin and A. W. Bushmaker, *ACS Nano*, 2015, **9**, 5372–5376.
114 M. Bobinger, P. L. Torraca, J. Mock, M. Becherer, L. Cattani, D. Angeli, L. Larcher and P. Lugli, *IEEE Trans. Nanotechnol.*, 2018, **17**, 940–947.
115 G.-Y. Gou, M. L. Jin, B.-J. Lee, H. Tian, F. Wu, Y.-T. Li, Z.-Y. Ju, J.-M. Jian, X.-S. Geng, J. Ren, Y. Wei, G.-Y. Jiang, Y. Qiao, X. Li, S. J. Kim, M. Gao, H.-T. Jung, C. W. Ahn, Y. Yang and T.-L. Ren, *ACS Nano*, 2019, **13**, 12613–12620.
116 R. M. Ronchi, J. T. Arantes and S. F. Santos, *Ceram. Int.*, 2019, **45**, 18167–18188.
117 Z. Lin, G. Zhang, X. Xiao, C. Au, Y. Zhou, C. Sun, Z. Zhou, R. Yan, E. Fan, S. Si, L. Weng, S. Mathur, J. Yang and J. Chen, *Adv. Funct. Mater.*, 2022, **32**, 2109430.
118 J. T. Lee, B. C. Wyatt, G. A. Davis, Jr., A. N. Masterson, A. L. Pagan, A. Shah, B. Anasori and R. Sardar, *ACS Nano*, 2021, **15**, 19600–19612.
119 C. J. Zhang, S. Pinilla, N. McEvoy, C. P. Cullen, B. Anasori, E. Long, S.-H. Park, A. Seral-Ascaso, A. Shmeliov, D. Krishnan, C. Morant, X. Liu, G. S. Duesberg, Y. Gogotsi and V. Nicolosi, *Chem. Mater.*, 2017, **29**, 4848–4856.
120 M. Ankitha, N. Shabana, P. V. Vaishag and P. A. Rasheed, *J. Electroanal. Chem.*, 2023, **928**, 117088.
121 Y.-J. Wan, K. Rajavel, X.-M. Li, X.-Y. Wang, S.-Y. Liao, Z.-Q. Lin, P.-L. Zhu, R. Sun and C.-P. Wong, *Chem. Eng. J.*, 2021, **408**, 127303.
122 X. Zhao, H. Cao, B. J. Coleman, Z. Tan, I. J. Echols, E. B. Pentzer, J. L. Lutkenhaus, M. Radovic and M. J. Green, *Adv. Mater. Interfaces*, 2022, **9**, 2200480.
123 A. N. Kumar and K. Pal, *Mater. Adv.*, 2022, **3**, 5151–5162.
124 M. C. Krecker, D. Bukharina, C. B. Hatter, Y. Gogotsi and V. V. Tsukruk, *Adv. Funct. Mater.*, 2020, **30**, 2004554.
125 J. Zheng, Z. Yu, Y. Wang, Y. Fu, D. Chen and H. Zhou, *ACS Nano*, 2021, **15**, 17499–17507.
126 J. Meriaux, M. Boinet, S. Fouvry and J. C. Lenain, *Tribol. Int.*, 2010, **43**, 2166–2174.
127 J. Wu, Y. Yu and G. Su, *Nanomaterials*, 2022, **12**, 828.
128 P. Sharma, S. A. Imtiaz and E. Rodriguez-Villegas, *Sci. Rep.*, 2019, **9**, 20079.
129 C. Cai, M. Hu, X. Ma, K. Peng and J. Liu, *IEEE Internet Things J.*, 2019, **6**, 3164–3174.
130 J. Audu, R. R. Dinrifo, A. Adegbenjo, S. P. Anyebe and A. F. Alonge, *Heliyon*, 2023, **9**, e14567.
131 A. M. Seddon, S. J. Richardson, K. Rastogi, T. S. Plivelic, A. M. Squires and C. Pfrang, *J. Phys. Chem. Lett.*, 2016, **7**, 1341–1345.
132 M. Wu, Z. Mao, K. Chen, H. Bachman, Y. Chen, J. Rufo, L. Ren, P. Li, L. Wang and T. J. Huang, *Adv. Funct. Mater.*, 2017, **27**, 1606039.
133 M. Asad and M. H. Sheikhi, *Sens. Actuators, B*, 2014, **198**, 134–141.
134 A. Huhle, D. Klaue, H. Brutzer, P. Daldrop, S. Joo, O. Otto, U. F. Keyser and R. Seidel, *Nat. Commun.*, 2015, **6**, 5885.
135 K. Zhu, K. Han, T. Carmon, X. Fan and G. Bahl, *Eur. Phys. J.: Spec. Top.*, 2014, **223**, 1937–1947.
136 M. Miansari and J. R. Friend, *Adv. Funct. Mater.*, 2016, **26**, 7861–7872.
137 X. Wang, D. R. Bauer, R. Witte and H. Xin, *IEEE Trans. Biomed. Eng.*, 2012, **59**, 2782–2791.
138 X. Zhou, J. Wen, Z. Wang, X. Ma and H. Wu, *J. Mater. Sci. Technol.*, 2022, **115**, 148–155.